

Geochemistry, Geophysics, Geosystems



RESEARCH ARTICLE

10.1029/2021GC009665

Decadal Geomagnetic Secular Variations From Greigite Bearing Dead Sea Sediments

Yael Ebert¹ , Ron Shaar¹ , and Mordechai Stein^{1,2}

¹The Institute of Earth Sciences, the Hebrew University of Jerusalem, Jerusalem, Israel, ²Geological Survey of Israel, 32 Yashayahu Leibowitz St., Jerusalem, Israel

Key Points:

- Rock and paleomagnetic data at decadal resolution from three coeval radiocarbon-dated late-Holocene sections of the Dead Sea, Israel
- Paleomagnetic data from sediments with high greigite content are compatible with archeomagnetic data
- Smoothing and inclination shallowing of the paleomagnetic data carried by greigite are negligible

Supporting Information:

Supporting Information may be found in the online version of this article.

Correspondence to:

Y. Ebert,
yael.ebert@mail.huji.ac.il

Citation:

Ebert, Y., Shaar, R., & Stein, M. (2021). Decadal geomagnetic secular variations from greigite bearing Dead Sea sediments. *Geochemistry, Geophysics, Geosystems*, 22, e2021GC009665. <https://doi.org/10.1029/2021GC009665>

Received 19 JAN 2021

Accepted 2 APR 2021

© 2021. The Authors.

This is an open access article under the terms of the [Creative Commons Attribution-NonCommercial-NoDerivs License](https://creativecommons.org/licenses/by-nc-nd/4.0/), which permits use and distribution in any medium, provided the original work is properly cited, the use is non-commercial and no modifications or adaptations are made.

Abstract Archeomagnetic data from the Levant revealed periods within the Holocene with fast and extreme changes in the geomagnetic field. Yet, the availability of the archeomagnetic data is sporadic and the correlation with the available sedimentary records from the region is rather poor. To further explore decadal variations in the directions of the field, we investigate three outcrops of the late Holocene Dead Sea that are exposed along the western retreating shores of the modern lake. The sediments were deposited under spatially varying limnological-environmental conditions, influencing their magnetic properties. The southern section, located near Ein-Gedi Spa (EG section) is dominated by detrital titanomagnetite whereas the northern sections, Nahal Og (Og section) and Ein-Feshkha (EF section), are dominated by authigenic greigite. The chronology of the sections was established by radiocarbon dating of short lived organic debris. The magnetic data were obtained in a 2 cm resolution. The EF section, spanning the time interval from ca. 2,500 cal yr BP to ca. 1,000 cal yr BP, is dominated by greigite and thus providing the most robust geomagnetic record with precise paleomagnetic directions. Greigite forms very early in the sediment and the effects of smoothing and the inclination shallowing are negligible. The new data reveal a maximal deviation of 20° from the geocentric axial dipole field between 2,400 to 2,200 cal yr BP accompanied with a fast swing in inclination from 60° to 35° over about a century. This suggests high geomagnetic field activity associated with the Levantine Iron Age geomagnetic anomaly.

1. Introduction

Archeomagnetic data from the Levant have provided valuable insights into the characteristics of geomagnetic secular variations, revealing previously unknown features such as jerks (Gallet et al., 2003), spikes (Ben-Yosef et al., 2009; Shaar et al., 2011), and a regional high field anomaly namely the Levantine Iron Age Anomaly (LIAA, Shaar et al., 2016, 2017). While archeomagnetic research has yielded large and valuable paleointensity data sets, the available archeomagnetic directions are relatively sparse and not continuous. This problem stems from the sporadic availability of in situ burnt archeological materials that were used in the archeomagnetic research. To complement archeomagnetic data, continuous, well-dated, high-precision, high-resolution sedimentary records are required. Sedimentary lacustrine records are potential targets for obtaining these objectives, mainly because they are typically continuous and potentially datable by radiogenic methods. Indeed, several paleomagnetic records were constructed from data retrieved from late Pleistocene and Holocene records of lakes occupying the tectonic depressions of the Dead Sea and Kinnerot basins, for example, Lake Lisan (Marco et al., 1998); Lake Kinneret (Thompson et al., 1985), Birket Ram Ma'ar (Frank et al., 2002), and Holocene Dead Sea (Frank et al., 2007a). Yet, when combined, the sedimentary lacustrine data display some inconsistencies (Shaar et al., 2018). Moreover, when the sections were recovered by drilling, the cores were not azimuthally oriented. In addition, it is not clear as to what degree inclination shallowing and smoothing mechanisms affect the recorded paleomagnetic directions in the sediments.

Here, we explore the secular variation of three contemporaneous radiocarbon-dated sections of the late Holocene Dead Sea (the upper part of the Ze'elim Fm.). The paleomagnetic study is based on detailed rock-magnetic analysis that identifies the main magnetic carriers and reveals the mechanism by which the magnetic remanence was acquired. With the new data, we aim to assemble a continuous, precise, high-resolution secular variation record for the Levant.

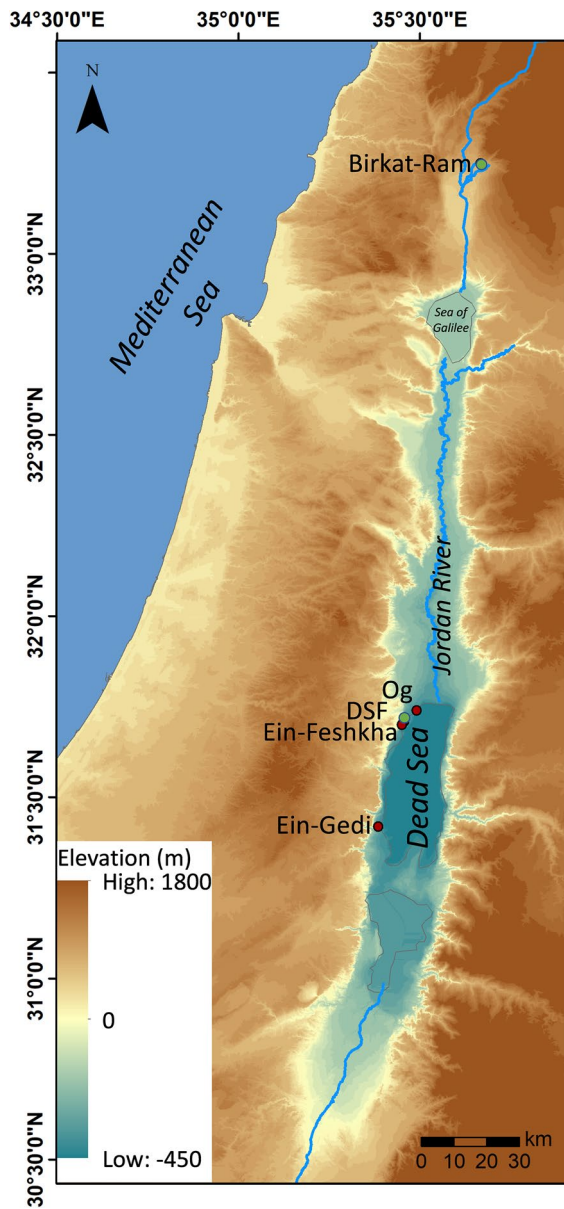


Figure 1. Location map of investigated outcrops and previous studies; red circles indicate sampling site locations along the Dead Sea, from north to south: Nahal Og (Og) (31.7400°E; 35.49029°N), Ein-Feshkha Nature Reserve (EF) (31.70839°E; 35.45524°N), and Ein-Gedi Spa (EG) (31.41917°E; 35.38486°N) (Figure 1). At each outcrop, we dug a vertical cross-section to reveal fresh sediment and collected 4–5 oriented samples per horizon using nonmagnetic plastic boxes (23 × 23 × 19 mm, Figure S1). In Ein-Feshkha and Og, the base of the sampled section was a thick layer of shoreline deposits representing a low stand of the lake dated to ~3,200–3100 BP (Bookman et al., 2004; E. Kagan et al., 2011; Migowski et al., 2006). This paleoshoreline marker was not found at Ein-Gedi section. The thickness of the investigated sections is: 3.15, 4.6, and 2.6 m for Og, Ein-Feshkha, and Ein-Gedi sections, respectively. A total of 448, 951, and 634 samples were collected from Og, Ein-Feshkha, and Ein-Gedi sections, respectively. Additional 12 samples for thermal demagnetization were collected from Ein-Gedi and Ein-Feshkha sections at selected heights, using quartz cylinders, 2.54 cm in diameter.

1.1. Geological and Limnological Setting

The modern and Holocene Dead Sea occupies the tectonic depression of the Dead Sea Basin that is located along the Dead Sea Transform fault (Garfunkel, 1981, Figure 1). The Dead Sea comprises a terminal hypersaline lake filled by a unique Ca-chloride brine solution that accommodates deposition of primary minerals such as aragonite and gypsum upon the supply of freshwater loaded with sulfate and bicarbonate to the lake (e.g. Belmaker et al., 2019; Stein et al., 1997). The lake receives also fine detritus sediments that are washed to it by the annual floods (e.g., Haliva-Cohen et al., 2012). Sedimentation rates vary from 2 to 3 mm/year (E. Kagan et al., 2011; Migowski et al., 2004). The Holocene Ze'elim formation comprises sequences of silty detrital sediments, the *ld facies* (laminated detritus) (Haliva-Cohen et al., 2012) consisting of quartz and calcite as major minerals interbedded with sequences of aragonite and detritus laminae the *aad facies* (alternating aragonite and detritus) (Machlus et al., 2000). The Dead Sea sediments contain two dominant magnetic minerals: titanomagnetite and greigite (Ebert et al., 2018, 2020; Frank et al., 2007a, 2007b; Ron et al., 2006). Titanomagnetite is transported to the lake by fluvial and alluvial systems, carrying a detrital remanent magnetization (DRM). Greigite is a diagenetic product of sulfate reducing bacteria (SRB) activity, carrying a chemical remanent magnetization (CRM). Ebert et al. (2020) investigated the processes governing the formation of greigite in the Holocene sediment and showed that iron and sulfate microbial reduction controls its precipitation. They measured reactive iron and sulfate in the pore fluids and concluded that the microbial activity associated with greigite precipitation is controlled by the availability of organic matter and reactive iron, which depends on freshwater input. Thus, sediments located closer to the Jordan River contain higher content of greigite.

2. Methods

2.1. Sampling

The sampling sections are located at gullies formed during the recent retreat of the modern Dead Sea. The sections from north to south are: Nahal Og (Og) (31.7400°E; 35.49029°N), Ein-Feshkha Nature Reserve (EF) (31.70839°E; 35.45524°N), and Ein-Gedi Spa (EG) (31.41917°E; 35.38486°N) (Figure 1). At each outcrop, we dug a vertical cross-section to reveal fresh sediment and collected 4–5 oriented samples per horizon using nonmagnetic plastic boxes (23 × 23 × 19 mm, Figure S1). In Ein-Feshkha and Og, the base of the sampled section was a thick layer of shoreline deposits representing a low stand of the lake dated to ~3,200–3100 BP (Bookman et al., 2004; E. Kagan et al., 2011; Migowski et al., 2006). This paleoshoreline marker was not found at Ein-Gedi section. The thickness

of the investigated sections is: 3.15, 4.6, and 2.6 m for Og, Ein-Feshkha, and Ein-Gedi sections, respectively. A total of 448, 951, and 634 samples were collected from Og, Ein-Feshkha, and Ein-Gedi sections, respectively. Additional 12 samples for thermal demagnetization were collected from Ein-Gedi and Ein-Feshkha sections at selected heights, using quartz cylinders, 2.54 cm in diameter.

2.2. Magnetic Measurements

The paleomagnetic procedures for all samples were as follows: measurements of the mass-specific susceptibility (χ) in 200 A/m field at 976 Hz; measurements of the natural remanent magnetization (NRM);

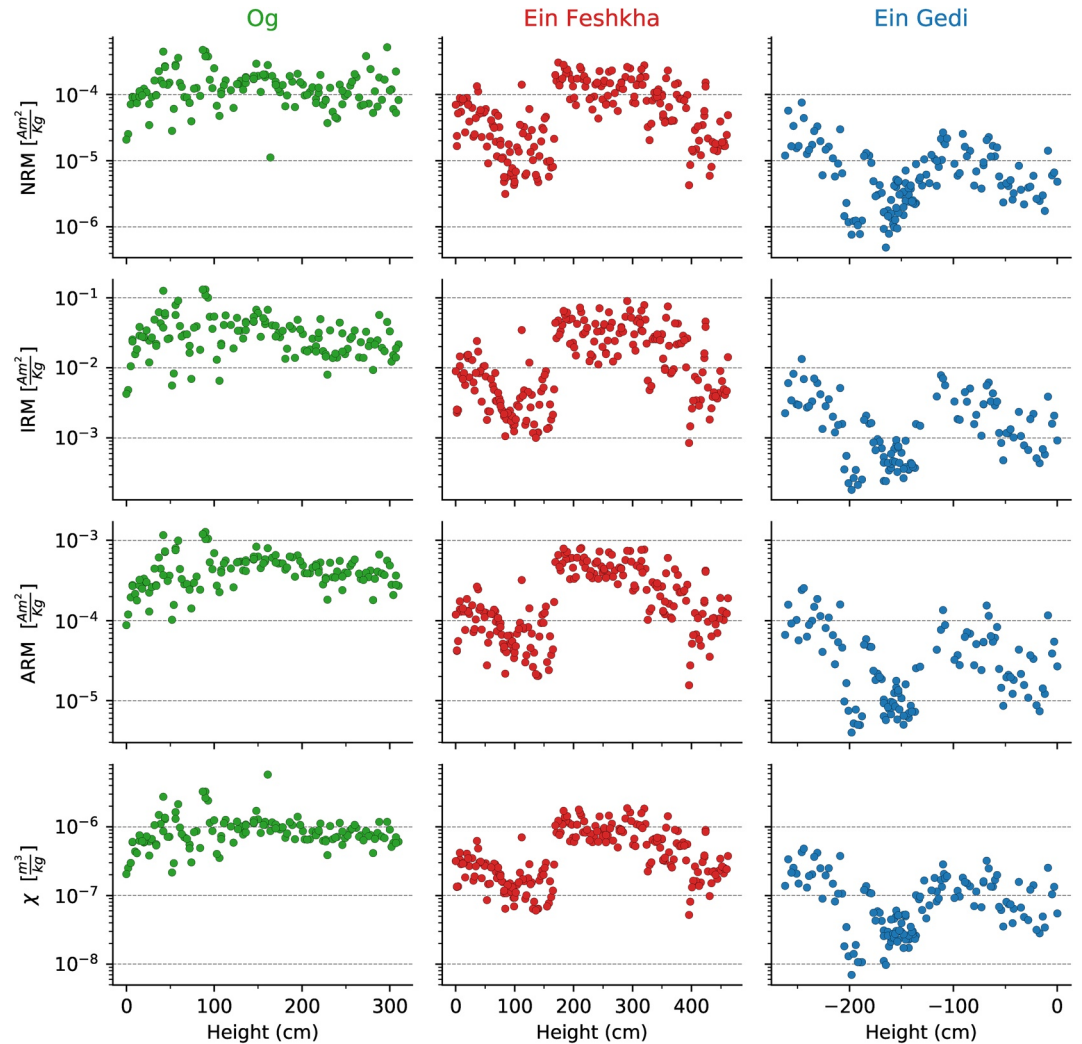


Figure 2. Depth profiles of mineral magnetic data: NRM, IRM, ARM, and susceptibility (χ), for each outcrop. Green, red, and blue denote Og, Ein-Feshkha (EF), and Ein-Gedi (EG), respectively. Trends of changes in natural remanent magnetization (NRM), isothermal remanent magnetization (IRM), anhysteretic remanent magnetization (ARM), and χ are similar at each outcrop.

stepwise alternating field (AF) demagnetization in 11 steps from 5 mT upto 110 mT; anhysteretic remanent magnetization (ARM) acquisition with a 0.1 mT DC bias field and 100 mT AF field along the z -axis of the sample; AF demagnetization of the ARM using the same steps used for the NRM demagnetization; isothermal remanent magnetization (IRM) acquisition in a 1,500 mT field along the z -axis of the sample followed by backfield IRM in a 300 mT field applied along the $-z$ direction. In addition, 10 samples from Ein-Gedi and Ein-Feshkha sections were demagnetized thermally with 16 steps from 100°C to 600°C. The demagnetization data were analyzed using the Demag GUI program, which is part of the PmagPy software package (Tauxe et al., 2016). Characteristic remanent magnetization (ChRM) was calculated from principal component analysis (PCA) (Kirschvink, 1980). The statistics MAD (maximum angular deviation, Kirschvink, 1980) and DANG (deviation angle, Tauxe & Staudigel, 2004) are used to characterize the quality of the ChRM. The MAD is a measure of the scatter of the of the data points about the least squares line and the DANG is the angle between a line connecting the center of mass and the origin and the least squares line. Sites (horizons) means and paleomagnetic statistics were calculated following Fisher (1953). S-ratio was calculated using the IRM measurements as $0.5 \times (1 - [\text{IRM}_{-300 \text{ mT}}/\text{SIRM}_{1500 \text{ mT}}])$ after Bloemendal et al. (1992). NRM, AF demagnetizations, ARM, and χ were measured not more than few days after the samples were collected and stored in a refrigerator.

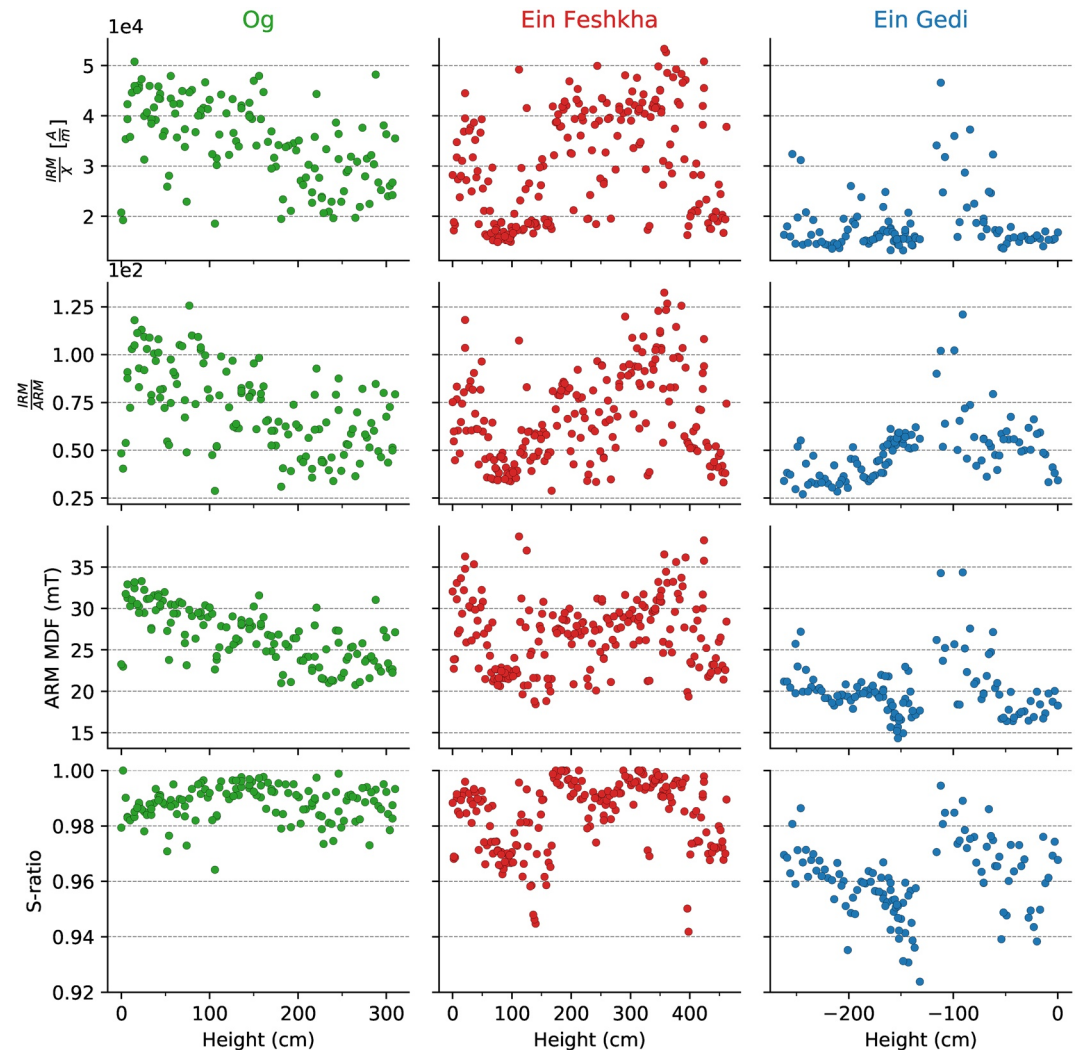


Figure 3. Depth profiles of mineral magnetic data: isothermal remanent magnetization (IRM)/ χ , IRM/ARM, median destructive field (MDF) of anhysteretic remanent magnetization (ARM), and S-ratio for each outcrop. Green, red, and blue denote Og, Ein-Feshkha (EF), and Ein-Gedi (EG), respectively. Changes in IRM/ χ , IRM/ARM, MDF of ARM and S-ratio indicate changes in the content of greigite at the outcrops. Og is characterized with high content of greigite, EF have section with higher content of greigite (170–320 cm) while in Ein-Gedi titanomagnetite is the dominant magnetic mineral.

NRM measurements and AF demagnetizations were done using a 2G Enterprises superconducting rock magnetometer (SRM) 750 or using a 2G Enterprises RAPID SRM, both equipped with inline two-axis AF demagnetizer coils; ARM was acquired and measured using the RAPID system. IRM was acquired using an ASC pulse magnetizer and was measured using an AGICO JR-6A dual speed spinner magnetometer at the Geological Survey of Israel, Jerusalem. Low field magnetic susceptibility (χ) was measured using an AGICO MFK-1 Kappabridge system. Magnetic analyses were done at the paleomagnetic laboratory at the Institute of Earth Sciences, The Hebrew University of Jerusalem.

2.3. Radiocarbon Dating

Radiocarbon ages were measured on 18 samples of short-lived organic debris, mostly small pieces of twigs, sampled directly from the sediment: three from Og section, eight from Ein-Feshkha section, and seven from Ein-Gedi section. The samples were measured at the Accelerator Mass Spectrometry (AMS) at the Radiocarbon laboratory, Weizmann Institute, Rehovot, Israel. Calibrated ages and age-depth Bayesian models were

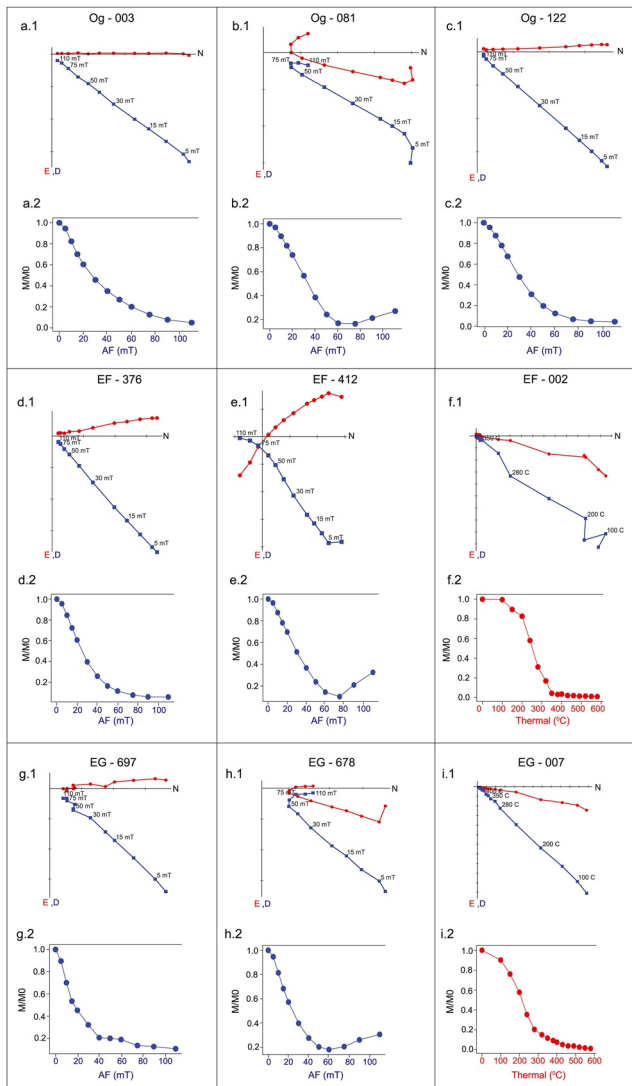


Figure 4. Representative orthogonal projection (Zijderveld diagram) and demagnetization curves (M/M_0) of demagnetized sediments samples from the three sites: (a–c) Og, (d–f) Ein Feshkha, and (g–i) Ein Gedi. Blue squares represent projection of the inclination on north-down plane. Red circles represent projection of the declination on north-east plane. (f and i) Representative plots of thermally demagnetized samples.

from Ein-Gedi section (dominated by titanomagnetite) show much more scattered Zijderveld diagrams with higher MAD and DANG values (Figures 4 and 5). Our acceptance criteria for the PCA directions are $MAD < 6^\circ$ and $DANG < 6^\circ$. In Og and Ein-Feshkha sections, all samples passed the criteria. At Ein-Gedi section, 25 samples out of the 634 did not pass the criteria. The reason for this difference is discussed below. Also, samples with high susceptibility have lower MAD and DANG (Figures 5a and 5b) and record the paleomagnetic directions at a higher precision.

Thermal demagnetization curves from Ein-Feshkha and Ein-Gedi (Figure 4f2 and 4i2 respectively) are in agreement with the conclusions of Ebert et al. (2020), showing low blocking temperature of $\sim 350^\circ\text{C}$ for the greigite-bearing sediments of Ein-Feshkha and higher blocking temperature range, from $\sim 350^\circ\text{C}$ to 550°C , for the titanomagnetite-bearing sediments in Ein-Gedi. Acquisition of a gyroremanent magnetization (GRM) during AF demagnetization (e.g., Sagnotti & Winkler, 1999; Snowball, 1997) was observed only

calculated using OxCal 4.3.2 program (Ramsey, 2008, 2009, 2017), using the IntCal13 calibration curve (Reimer et al., 2013).

3. Results

3.1. Rock-Magnetic Measurements

The magnetic properties of Og, Ein-Feshkha and Ein-Gedi sediments were investigated in detail by Ebert et al. (2020). They compared the bulk magnetic parameters (χ , ARM, IRM) with electron microscopy analysis, first order reversal curves (FORC) and pore-fluids composition. Here, we present additional analyses. Figure 2 shows depth profiles of NRM, IRM, ARM, and χ . Figure 3 displays ratios of IRM/χ , IRM/ARM , and S-ratio, as well as the median destructive field (MDF) of the ARM. The trends of changes in the bulk parameters (NRM, IRM, ARM, and χ) (Figure 2) are similar for each section, indicating that they reflect changes in the concentration and mineralogy of the ferrimagnetic phases. Ebert et al. (2020) suggested that the high values of magnetic parameters at Og and Ein-Feshkha sections (170–320 cm) correspond to high content of the mineral greigite; intermediate values of magnetic parameters, at Ein-Gedi section (0–120 and 200–260 cm) and at Ein-Feshkha section (0–170 and 320–460 cm), indicate lower content of greigite; and low magnetic parameters values at Ein-Gedi section (130–200 cm) are associated with dominance of the mineral titanomagnetite. The ratios and the MDF shown in Figure 3 are in agreement with these conclusions. Og and Ein-Feshkha sections (170–320 cm) have S-ratio values close to 1 and are characterized by higher IRM/χ values implying high concentration of greigite (Roberts, 1995; Sagnotti & Winkler, 1999; Snowball, 1991; Snowball & Thompson, 1990). Lower IRM/χ values and S-ratio values at Ein-Feshkha section (0–170 cm and 320–460 cm) are similar to the typical values in Ein-Gedi section and correspond to intervals with lower concentration of greigite. Also, the IRM/ARM and the MDF are higher in the Og and Ein-Feshkha sections compared to the values from the Ein-Gedi section.

3.2. Paleomagnetic Measurements

Figure 4 shows representative Zijderveld diagrams and demagnetization curves (M/M_0) from the three sections. Most of the samples demonstrate a stable paleomagnetic vector converging toward the origin. Samples from Og and Ein-Feshkha sections (rich in greigite) are characterized by low MAD (Kirschvink, 1980), typically less than 1.5° and low DANG (Tauxe & Staudigel, 2004), typically less than 2° (Figure 5). Samples

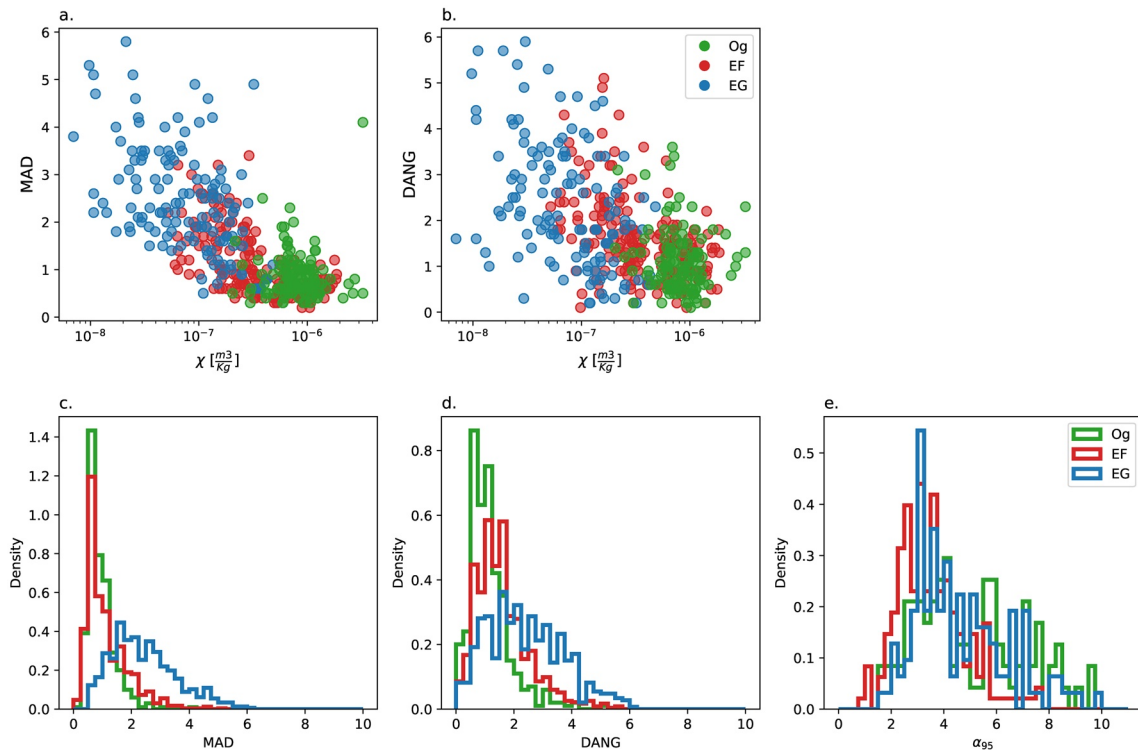


Figure 5. Quality and precision of the paleomagnetic data from the three outcrops. Green, red, and blue denote Og, Ein-Feshkha (EF), and Ein-Gedi (EG), respectively. (a, b) maximum angular deviation (MAD), deviation angle (DANG) versus susceptibility; samples with high greigite content and high χ (EF and Og) yielded lower values of MAD and DANG. (c, d, e) Histogram of the MAD, DANG of the samples; samples from EF and Og are characterized by lower MAD, DANG than EG. (e) α_{95} of horizons calculated by averaging of 4–5 samples per horizon; Samples from Ein-Feshkha have lowest α_{95} .

in few samples (Figures 4b, 4e, and 4h). However, most of the samples did not acquire a GRM and were characterized by stable linear vector converging to the origin up to 110 mT peak AF amplitude (Figures 4a1 and 4b1). This behavior of greigite that does not show GRM acquisition was also observed in other environments (Rowan & Roberts, 2006; Sagnotti et al., 2005)

Depth profiles of ChRM directions (inclination, declination) are shown in Figure 6. The inclination ranges in Og, Ein-Feshkha, and Ein-Gedi sections are 20°–50°, 30°–60°, and 30°–60°, respectively. The declination ranges in Og, Ein-Feshkha, and Ein-Gedi sections are –20°–20°, –20°–20°, and –20°–30°, respectively. These values are close to the expected geocentric axial dipole (GAD) direction in the Dead Sea, of inclination of 51° and 0° declination.

3.3. Age Models

Table 1 lists the results from radiocarbon dating. Ein-Feshkha and Ein-Gedi sections contain sufficient organic material for deposition age modeling. The Og section, however, is very poor in organic debris and the three samples could not provide a reliable deposition model. The age-depth models of Ein-Feshkha and Ein-Gedi sections were constructed using a Poisson Bayesian depositional model (P_sequence, [Ramsey, 2008]) with k factor of 1 and interpolation rate of 1 every 10 cm (0.1 cm^{-1}) as suggested by E. J. Kagan et al. (2010), E. Kagen et al. (2011), who constructed an age-depth model for a nearby exposed section (Figure 7). The OxCal codes are given in the supplementary material. The age-depth model of the lower part of the Ein-Feshkha section (below 200 cm) (Figure 7b) is defined by only two radiocarbon samples, thus we use an external age constraint that is derived from independent archeomagnetic data from the region. Shaar et al. (2016, 2018) identified anomalous steep inclinations in the regional magnetic field (>65°) between the tenth and the eighth centuries BCE that were associated with the Levantine iron age anomaly (LIAA at ~2,750 years cal BP). These data were used for “After” command in the OxCal code. The paleomagnetic directions in Ein-Feshkha section do not show such steep inclinations (Figure 6), which is consistent with

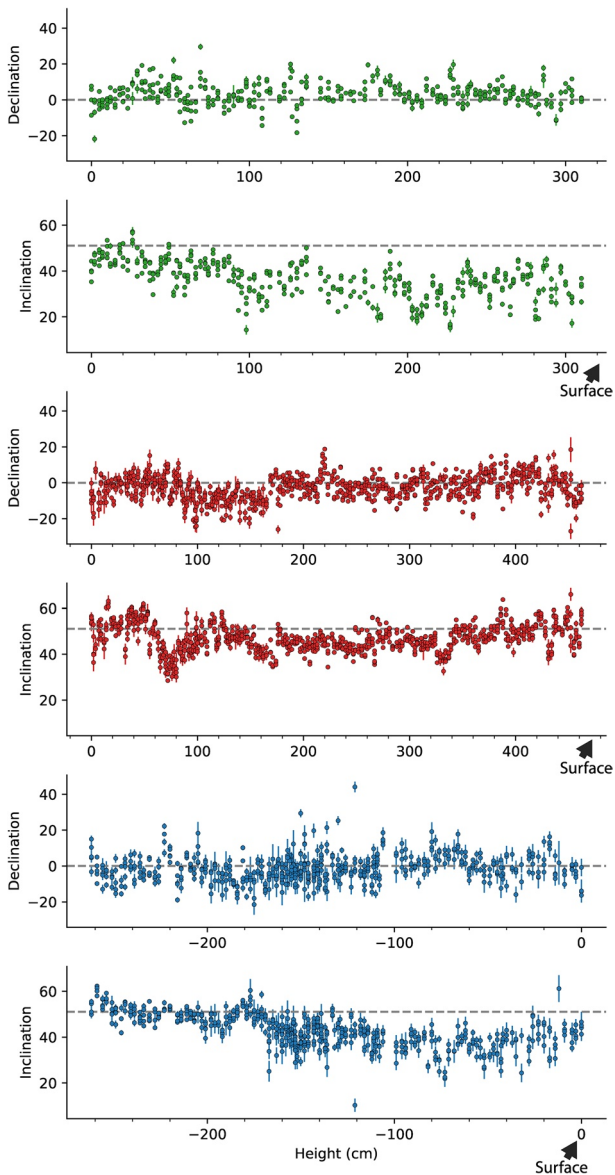


Figure 6. Depth profiles of declination and inclination for all the samples from each outcrop. Green, red, and blue circles denote Og, Ein-Feshkha (EF), and Ein-Gedi (EG), respectively. Error bars are calculated from samples maximum angular deviation (MAD). Gray dashed line represents the expected geocentric axial dipole (GAD) declination and inclination 0° and 51° , respectively.

inclinations of the two sections overlap, but the inclinations show some dissimilarities: the fast change in the inclination of the Ein-Feshkha sediments between 2,500 and 2,400 cal yr BP is not observed in the Ein-Gedi section and the inclinations of the Ein-Gedi sediments are much shallower than those of Ein-Feshkha after 2,000 cal yr BP. The inclination difference in the lower part of Ein-Gedi section can be explained by the geochemical pore-fluids measurements that showed a clear influence of Ein-Qedem spring brine (Ebert et al., 2020), which might have caused a secondary magnetization. The lower inclination of the upper part of Ein-Gedi section suggests that this section, which is poor in greigite, is more affected by inclination shallowing and smoothing. In addition, the MAD, DANG, and α_{95} are smaller in the Ein-Feshkha sediments than in Ein-Gedi (Figures 5c–5e). The differences between the paleomagnetic properties in Ein-Feshkha

their age being younger than 2,750 cal yr BP. In addition, two age model boundaries separating between units with different sedimentation rates were defined for the Ein-Feshkha age-depth model. These boundaries match times of significant changes in the lake hydrolimnological history that limit a period of lake level rise accompanied by an increase in sediment accumulation between 170 and 396 cm (Ebert et al. 2020). For the age-depth model of the Ein-Gedi section (Figure 7c), we only added the “After” command at 2,750 cal yr BP.

The age models of Ein-Feshkha and Ein-Gedi sections span the time interval from $\sim 2,700$ to $\sim 1,200$ cal yr BP (Figure 7). There are some variations in the sedimentation rate between and within the sections. The upper part of Ein-Feshkha (470–396 cm) has the lowest sedimentation rate in Ein-Feshkha of 0.20 cm/yr. The middle section of Ein-Feshkha (396–170 cm), which was accumulated during lake level rise (Ebert et al., 2020), is characterized by a high sedimentation rate of 0.40 cm/yr. The base of section (0–170 cm) has an average sedimentation rate of 0.28 cm/yr, similar to the rate calculated by E. Kagan et al. (2011), who dated a nearby section. The averaged sedimentation rate in the entire Ein-Feshkha section is 0.31 cm/yr. The averaged sedimentation rate in Ein-Gedi is 0.15 cm/yr, much lower than in Ein-Feshkha and similar to the rate calculated by Migowski et al. (2004) for the DSEn core collected in the region of Ein-Gedi. The large difference in the sedimentation rates of the two sections probably reflects the distance from the main detrital supply to the Dead Sea, the Jordan River (Figure 1).

4. Discussion

4.1. Paleomagnetic Recording by Greigite

Paleomagnetic directions were retrieved from the late Holocene sections that are exposed in the marginal terraces of the Dead Sea at Ein-Gedi Spa and Ein-Feshkha Nature Reserve. The chronology of the sections was achieved by radiocarbon dating of short lived radiocarbon debris, suggesting that the ages of the studied sedimentary sequences lie between $\sim 2,700$ and $\sim 1,200$ cal yr BP (Figure 7). Samples were taken and analyzed also from Nahal Og section (Figure 1), yet no solid chronology is available for the Og data (Figure 7, supplementary Table S1) and therefore Og is not included in the following discussion.

Figure 8 shows the mean directions of Ein-Feshkha and Ein-Gedi sections, where each data point represents an average of 4–5 samples per horizon. The smoothed curves in Figure 8 are calculated by averaging samples in a 50, 60 years running window for Ein-Feshkha and Ein-Gedi samples, respectively. The number of samples in each window is typically 20–45 for Ein-Feshkha and 10–35 for Ein-Gedi. The data used to generate Figure 8 is given in Tables S2 and S3, supplementary material. The declinations of the two sections overlap, but the inclinations show some dissimilarities: the fast change in the inclination of the Ein-Feshkha sediments between 2,500 and 2,400 cal yr BP is not observed in the Ein-Gedi section and the inclinations of the Ein-Gedi sediments are much shallower than those of Ein-Feshkha after 2,000 cal yr BP.

Table 1
Radiocarbon Data

Sample name	Lab ID	Height (cm)	¹⁴ C years (BP)	Calibrated age (68% probability)	Calibrated age (95% probability)	Modeled age (68% probability)	Modeled age (95% probability)
Ein Feshkha site							
Boundary (Bottom)		0				2,753–2681 BP	2,753–2534 BP
YE6	RTD10047	60	2,518 ± 41	2,734–2,502 BP	2,747–2466 BP	2,546–2486 BP	2,562–2366 BP
YE4	RTD10046	161	2,178 ± 35	2,303–2,133 BP	2,311–2114 BP	2,179–2073 BP	2,244–2,043 BP
*YE5	RTD 10045	226	2,223 ± 30				
YE7	RTD10044	246	1,912 ± 30	1,885–1,825 BP	1,931–1,741 BP	1,928–1,871 BP	1,950–1,846 BP
YE8	RTD10043	304	1,833 ± 29	1,815–1,735 BP	1,865–1,702 BP	1,789–1,733 BP	1,818–1,714 BP
YE9	RTD10042	401	1,626 ± 29	1,561–1421 BP	1,599–1,414 BP	1,559–1,448 BP	1,568–1,431 BP
YE10	RTD10041	416	1,579 ± 30	1,524–1,415 BP	1,540–1,403 BP	1,471–1,414 BP	1,497–1,393 BP
YE13	RTD10040	447	1,373 ± 29	1,311–1,282 BP	1,341–1,271 BP	1,312–1,282 BP	1,343–1,271 BP
Boundary (Surface)		470				1,238–1,148 BP	1,285–1,090 BP
Og site							
YE14	RTD10050	12	2,494 ± 53	2,720–2,490 BP	2,741–2,379 BP		
YE16	RTD10049	113	1,966 ± 26	1,945–1,884 BP	1,989–1,868 BP		
YE15	RTD10048	257	1,934 ± 30	1,923–1,830 BP	1,949–1,820 BP		
Ein-Gedi site							
Boundary (Bottom)		–260				2,753–2,717 BP	2,753–2673 BP
YE2	RTD10039	–147	2,293 ± 30	2,350–2,310 BP	2,355–2,180 BP	2,189–2,155 BP	2,220–2,151 BP
EG1-RC16	RTD8922	–144	2,153 ± 26	2,298–2,113 BP	2,305–2,048 BP	2,157–2,134 BP	2,180–2,120 BP
YE1	RTD10038	–124	2,029 ± 30	2,036–1,931 BP	2,102–1,898 BP	2,040–1,987 BP	2,059–1,971 BP
EG1-RC15	RTD8923	–108	1,998 ± 26	1,988–1,904 BP	1,998–1,889 BP	1,942–1,896 BP	1,967–1,882 BP
EG1-RC5	RTD8919	–12	1,340 ± 23	1,295–1,271 BP	1,304–1187 BP	1,296–1,276 BP	1,305–1260 BP
*EG1-RC7	RTD8920	–26	1,768 ± 27				
*EG1-RC9	RTD8921	–81	1,627 ± 24				
Boundary (Surface)		0				1,221–1,168 BP	1,241–1,132 BP

Outlier are marked with asterisk (*).

and Ein-Gedi sections are likely a result of their different magnetic mineralogy. Ebert et al. (2020) showed that the dominant magnetic mineral in the Ein-Feshkha section is greigite, whereas in the Ein-Gedi section the dominant mineral is titanomagnetite. Accordingly, the two sections encompass different recording mechanisms: DRM at Ein-Gedi section versus CRM at Ein-Feshkha section. The CRM (greigite-bearing sediments) apparently records the paleomagnetic direction in better precision than the DRM (titanomagnetite-bearing sediments) since the former is not affected by inclination shallowing (Figure 8), demonstrates a more stable primary magnetization (Figures 4 and 5) and shows the lowest data scatter within horizons (Figures 5e, 6, and 8). Thus, we conclude that the Ein-Feshkha sediments comprise the most robust recorder of the paleomagnetic direction in the studied Dead Sea region.

The Ein-Feshkha section yields a decadal resolution secular variation record covering 1,500 years from ~2,700 to ~1,200 cal yr BP. In addition to the high temporal resolution of Ein-Feshkha section, its greigite-bearing record has some advantages over the other available sediment core records from the region. Figure S2, supplementary material, compares the inclination from Ein-Feshkha section (this study) with Ein-Feshkha DSF-B core (Frank et al., 2007a) and Birkat Ram core (Frank et al., 2002). The advantages of outcrop over core data are clear: an outcrop enables orienting the samples thus declinations are accurately measured; outcrops enable averaging more samples per horizon, increasing the precision of the paleomagnetic data. Figure 6 demonstrates the advantage of collecting more than one sample per horizon. Outliers

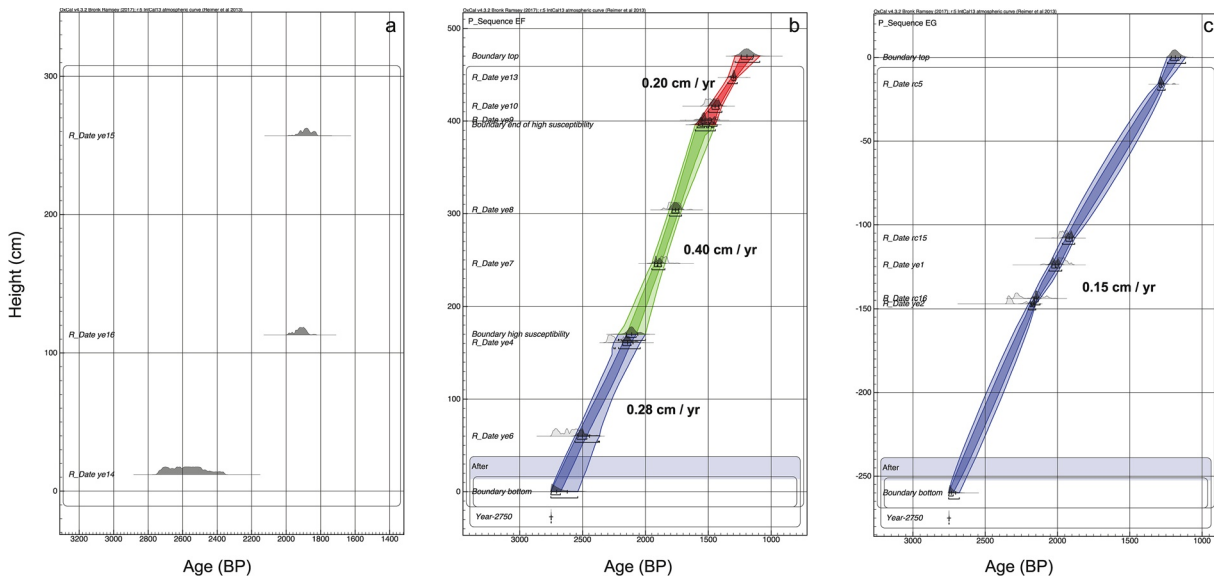


Figure 7. Radiocarbon ages and depth-age models of (a) Og, (b) Ein-Feshkha, and (c) Ein-Gedi. Light and dark colors of the age distributions in (b–c) show calibrated and modeled ages, respectively. The 68% and 95% probability density range of the depth-age model curves are shown in light and dark colors, respectively, where boundaries in (b) are shown with different colors. Outliers samples are not shown.

are evident several horizons, thus some dissimilarities between the core data and outcrop data can be explained by the presence of outliers in the core. All the above mentioned limitations of the core data also apply to the Birkat Ram core, with the addition of different sedimentation rate and sampling resolution of Birkat Ram (higher sedimentation rate at Ein-Feshkha section (average of ~ 0.31 cm/yr) compared to an average of ~ 0.12 cm/yr at Birkat Ram). In summary, the Ein-Feshkha section shows negligible inclination shallowing and smoothing. Therefore, we suggest that future paleomagnetic analysis of the Dead Sea sediments should be focused on greigite-bearing sections with similar properties as the Ein-Feshkha section.

The mean paleomagnetic directions that were retrieved from the Ein-Feshkha section are shown in Figure 9a together with the available archeomagnetic data (Shaar et al., 2018; Tema et al., 2018, 2021) from this time interval in a radius of 600 km around the study area. Most of the archeomagnetic data points scatter along the Ein-Feshkha curve, with only a few points that slightly deviate from the curve. We bear in mind that for the archeomagnetic samples individual radiocarbon ages were determined, while the Ein-Feshkha section chronology is based on age-depth Bayesian model (Figure 7). Both data sources have their uncertainties (e.g., in the radiocarbon ages and sedimentary lock-in depth) that could cause small shifts in the age of the data points, for example, at 2,500–2,400 cal yr BP and 1,950–2,200 cal yr BP. These differences are discussed in the following section. Nevertheless, the overall good correspondence between the archeomagnetic and the sedimentary data (e.g., inclination) suggests that inclination shallowing is negligible in the greigite bearing sediment. The fast inclination changes between 2,500 and 2,400 cal yr BP and the sharp change in declination around 2,000 cal yr BP suggest minor smoothing over several decades at the most.

4.2. Lock-In Depth

The comparison between Ein-Feshkha and the archeomagnetic data (Figure 9a) shows some apparent discrepancies between $\sim 1,950$ and 2,550 cal yr BP. Interestingly, a shift of the Ein-Feshkha record of about 200 years toward younger ages yields a nearly perfect synchronization between the two records and reduces the discrepancies to only a single data point at 1,300 cal yr BP (Figure 9b). This artificial “fix” raises the possibility of a delay in the magnetic recording mechanism, which may be related to lock-in depth.

A variety of depositional and post depositional processes can produce a time lag between the age of the sediments and the magnetic recording age. In Ein-Feshkha, this lag is associated with the depths at which the diagenetic microbial activity results in precipitation of greigite. Previous studies suggested that sulfate

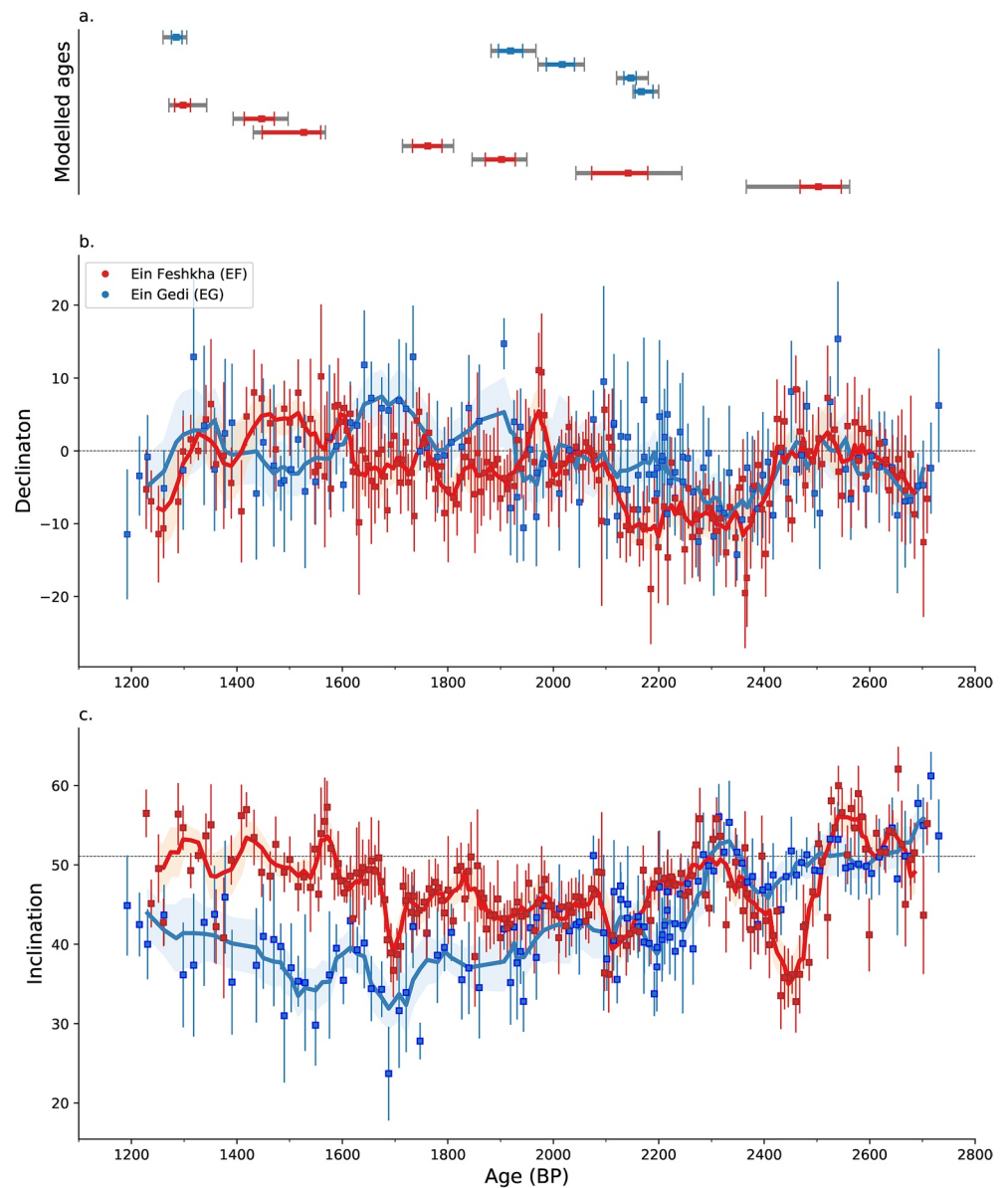


Figure 8. Mean declinations and inclinations of Ein-Feshkha (EF) and Ein-Gedi (EG) versus age. (a) Modeled ages at each site (Table 1). (b–c) Error bars are horizons mean directions calculated using 4–5 samples per horizon; errors are calculated from the α_{95} . The solid curve and the error envelopes are smoothed curves calculated by averaging samples over a running 50 (60) years window for EF (EG). Gray dashed line shows the expected geocentric axial dipole (GAD) declination and inclination: 0° and 51° , respectively. The declination curves overlap, while the inclinations in EG are shallower than EF after $\sim 2,000$ BP.

and iron reduction start instantly with sediment deposition in the upper 10 cm of the sediment column (Häusler et al., 2014; Nishri & Stiller, 1984). Porewaters extracted from the Ein-Feshkha sediments showed excess of reactive iron (0.26–1.44 mmol/kg (Fe^{2+})) and sulfate (3–6 mmol/L (SO_4^{2-})), indicating that greigite precipitation stops due to lack of labile organic matter (Ebert et al., 2020). The sulfate reduction rate (SRR) calculated by Häusler et al. (2014) for the modern Dead Sea in the top 12 cm of the sediment, indicates that sulfate reduction in the late Holocene environment of the shallow Dead Sea margin may be reduced to a minimum depth of a few dozens of centimeters below the lake's surface sediment. Considering the average sedimentation rate at the Ein-Feshkha section, this would yield an average delay of about several decades. We note that at the older part of the section (between $\sim 2,700$ and 2,400 cal yr BP), the uncertainty

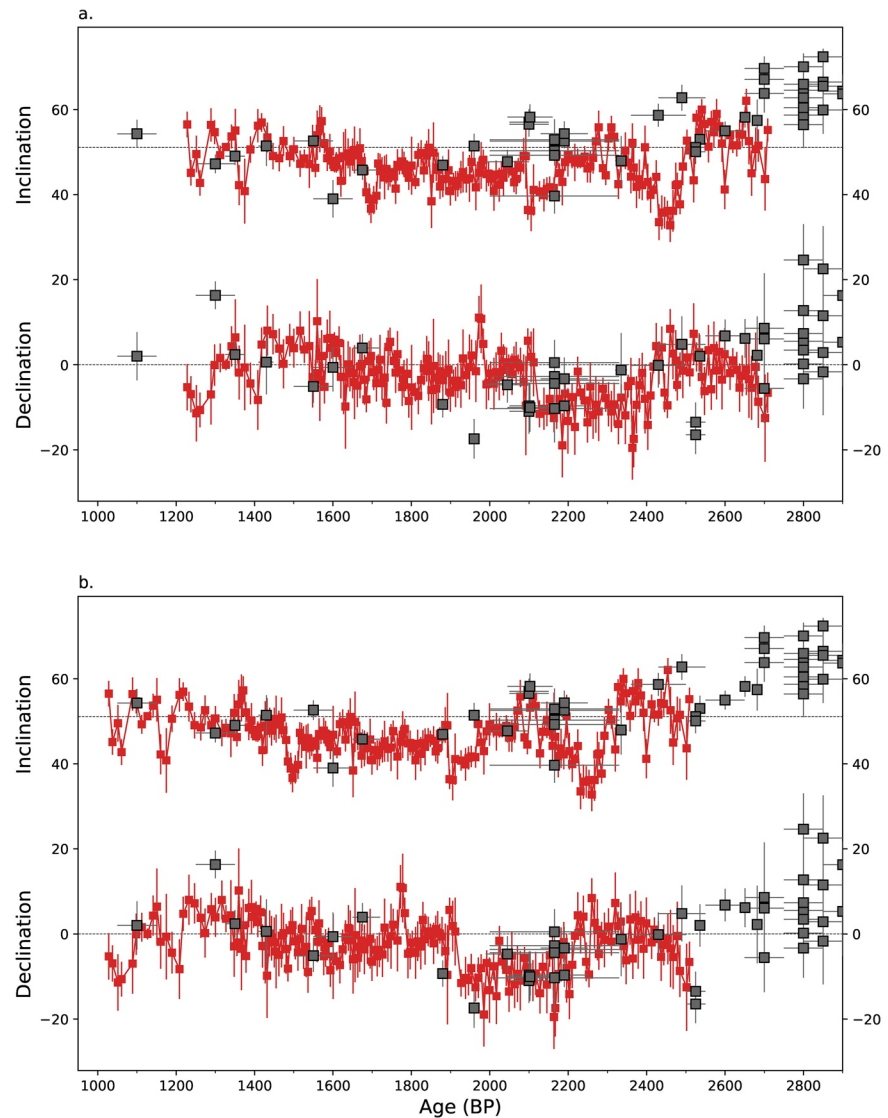


Figure 9. Comparison between sedimentary and archeomagnetic data. Mean directions of the horizons in Ein-Feshkha are shown in red; archeomagnetic data (Shaar et al., 2018; Tema et al., 2018, 2021) are shown in gray. Gray dashed lines represent the expected geocentric axial dipole (GAD) directions. (a) Ein-Feshkha (EF) data are plotted according to the depth-age model in Figure 7. There are some dissimilarities between the two data sets. (b) Compatibility between the sedimentary and the archeomagnetic data achieved after a shift of 200 years toward younger ages.

in the age-depth allows a larger shift of Ein-Feshkha age that together with the lock-in depth could yield a better synchronization between the archeomagnetic and sedimentary data during this time interval. In the following, in an effort to synchronize the two records as a mean to detect secular variation trends, we choose to apply a constant 200 years shift to the entire sedimentary age model as shown in Figure 9b. This artificial constant shift is a compromise that does not take into account the variations in the sedimentation rate and the different age uncertainties associated with the archeomagnetic data points and the sedimentary data. Instead, it uses the archeomagnetic data as fixed tie points. Nevertheless, it enables us to fill the gaps between the archeomagnetic data with the continuous high-resolution record of Ein-Feshkha. With more sedimentary and archeomagnetic data to be acquired in the future, we be able to further test this model and improve its dating.

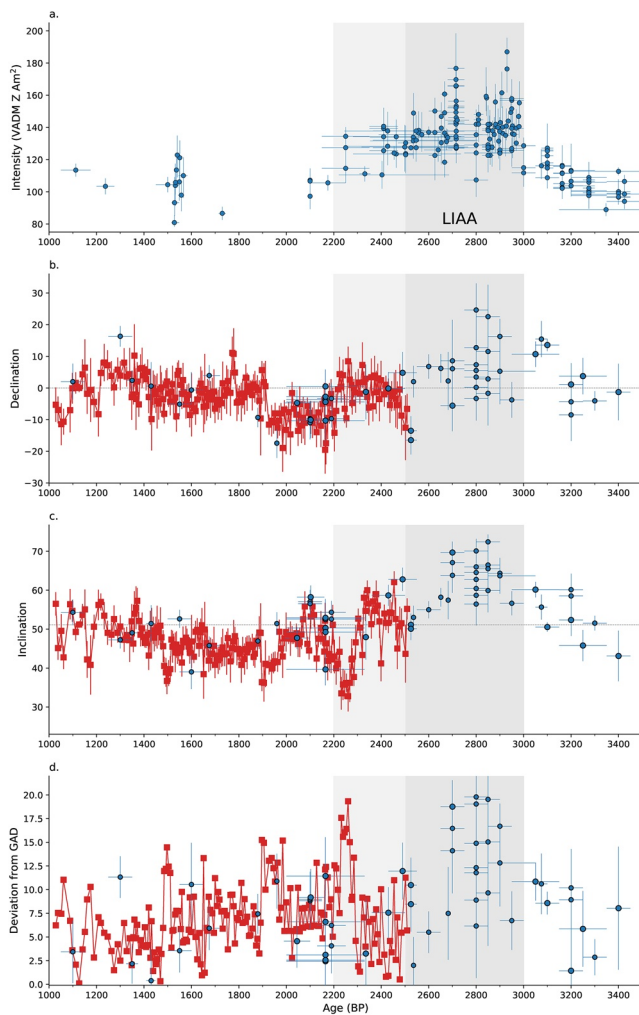


Figure 10. Paleomagnetic data from Ein-Feshkha (EF) (red squares) plotted together with archeomagnetic data (blue circles) from within a radius of ~ 600 km around the Dead Sea. (a) Paleointensity data from Israel (Ben-Yosef et al., 2017; Shaar et al., 2011, 2016; Vaknin et al., 2020), Jordan (Ben-Yosef et al., 2009), Syria (Gallet & Al-Maqdissi, 2010; Gallet et al., 2006, 2008, 2014; Genevey et al., 2003), and Cyprus (Shaar et al., 2015). (b–c) Declination and inclination from EF and from archeomagnetism (Shaar et al., 2018; Speranza et al., 2006; Tema et al., 2018, 2021; Vaknin et al., 2020). Fast change in the inclinations of EF is observed between 2,400 and 2,200 cal yr BP (d) Deviation from the geocentric axial dipole (GAD); a deviation of 20° appears in EF at $\sim 2,200$ yr BP, suggesting a later decaying of the LIAA.

the models display a general trend of decrease in declination between $\sim 2,800$ and 2,000 cal yr BP and in inclination between $\sim 2,800$ and $\sim 1,800$ cal yr BP. This trend in the paleomagnetic direction is consistent with the relatively fast change in VGP path obtained for high-latitude sediments from the NW Barents Sea in the Arctic (Caricchi et al., 2020) between 2,600 and 2,000 cal yr BP. The VGP path of Caricchi et al. (2020) also identified a VGP stand at relatively low latitudes around northern Europe during the early stages of the LIAA, which may explain the high inclinations observed in the Levant before the deposition of the Ein-Feshkha sediments.

4.3. Implications for Regional Geomagnetic Field Changes

Paleointensity data from the east Mediterranean-Levant (Cyprus, Syria, Israel, and Jordan) are compiled in Figure 10a (see references in Figure 10 caption), where we show only data obtained using paleointensity methods and age scales that were cross tested against each other (Shaar et al., 2020). The directional data (Figures 10b–10d) include data from Israel (Shaar et al., 2018), Cyprus (Tema et al., 2018, 2021), and Syria (Speranza et al., 2006). One of the most interesting features in the data presented in Figure 10 is the Levantine Iron Age Anomaly (LIAA) at 3,000 cal yr BP defined by Shaar et al. (2016, 2017) as a time interval with anomalously high field intensity and large angular deviation from GAD field. The onset of the LIAA is clear from the fast increase of the paleointensity data $\sim 3,000$ years BP (Figure 10a). However, the termination of the LIAA is less clear as the field intensity remained high for several centuries after the peak of the LIAA, and decayed gradually, at a much slower rate. Vaknin et al. (2020) suggested that the LIAA extended at least until 2,536 cal yr BP based on high field intensity values from historically dated burnt structure. This raises a question regarding the timing of the termination of the LIAA. The continuous Ein-Feshkha records contributes to this discussion. At the base of Ein-Feshkha section, the angular deviation from GAD is less than 10° . Yet, a fast change in the inclinations of Ein-Feshkha is observed between 2,400 and 2,200 cal yr BP, with a swing in inclination from $\sim 60^\circ$ to 35° over about a century and angular deviation from GAD reaching nearly 20° . This suggests that the time interval of the anomalous LIAA event can be extended to a longer duration and the activity of the geomagnetic field in the Levant gradually decayed after 2,200 cal yr BP.

Figure 11 shows the Ein-Feshkha data in comparison with predictions from global models of the Holocene geomagnetic field: ARCH3k.1 (Korte et al., 2009); ARCH10k.1, CALS10k.2, and HFM.OL1.A1 (Constable et al., 2016); pfm9k.1 (Nilsson et al., 2014); SHA.DIF.14k (Pavón-Carrasco et al., 2014); SHAWQ2k (Campuzano et al., 2019); SHAWQ-Iron Age (Osete et al., 2020) as well as the latest paleosecular variation (PSV) curve of the Middle East (Tema et al., 2021). We show in Figure 11 the smoothed Ein-Feshkha data (i.e. Figure 8) to enable a comparison with the inherent smoothed nature of the models. Considering the error envelope, the Ein-Feshkha data are generally in agreement with the models, except for the time interval of 2,200–2,400 cal yr BP and the positive declination around $\sim 1,400$ cal yr BP. The latter feature, which is undetected in the models is seen in the regional PSV curve. The general agreement between the PSV curves, field models and Ein-Feshkha, provides further support to the validity of the greigite-bearing sediments as paleosecular variation recorders. In a broad picture, both the Ein-Feshkha data and

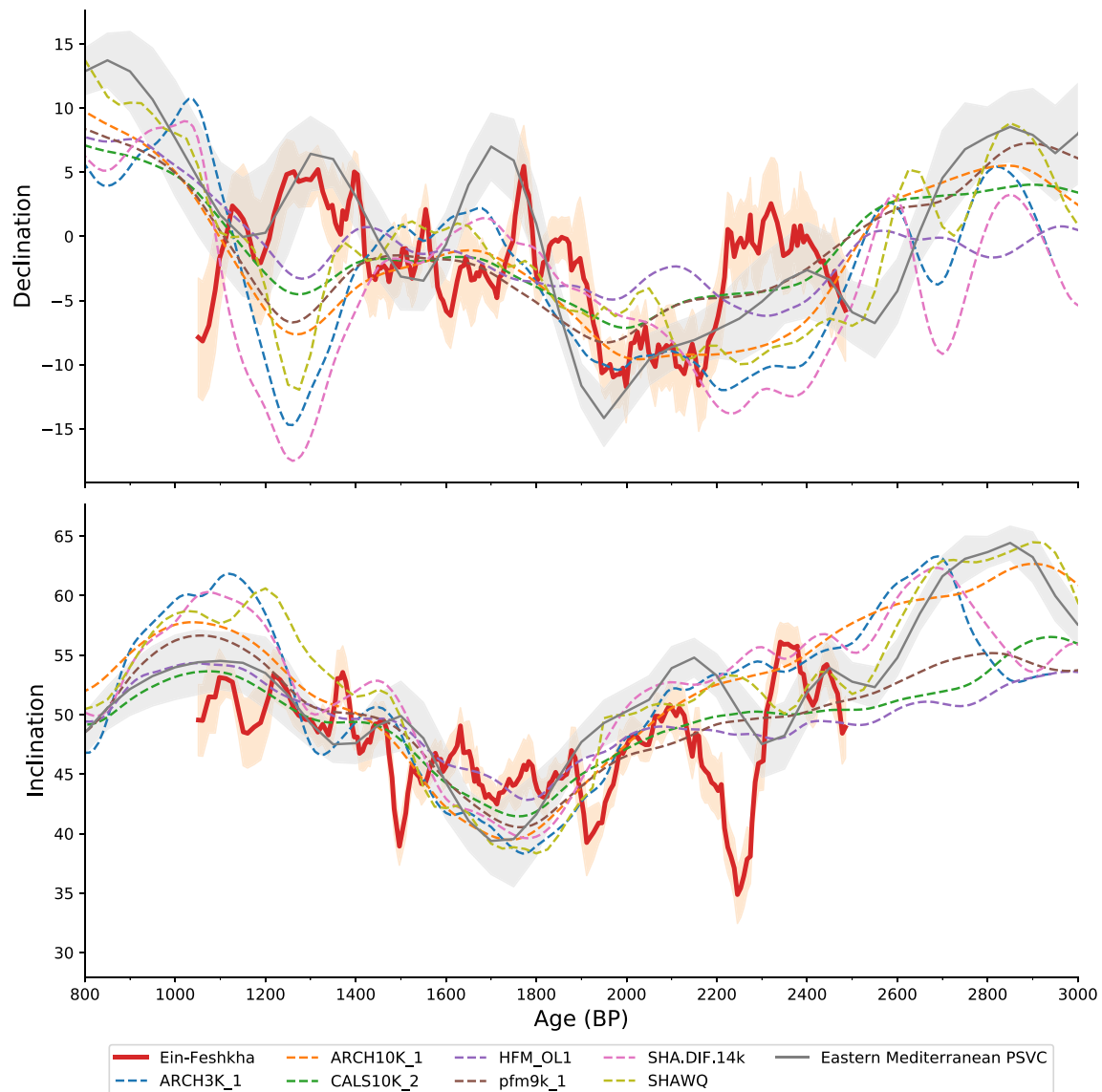


Figure 11. Comparison of the smoothed Ein-Feshkha (EF) curve (Figure 8) with predictions from global geomagnetic models at the location of EF and the Middle East paleosecular variation curve relocated to the location of EF. See text for reference list.

Data Availability Statement

All the paleomagnetic measurements and the interpretations are available at the MagIC database (earthref.org/MagIC/17107).

Acknowledgments

The authors thank Rami Weinberger for the use of his laboratory at the Geological Survey of Israel for conducting measurements. We thank Elisabetta Boaretto and Eugenia Mintz from Dangoor research accelerator mass spectrometry (D-REAMS) laboratory at the Weizmann Institute for all the help in preparing and measuring the ^{14}C samples. Yuval Burstein, Elan Levy, Jonatan Keinan, Nurit Weber, and Michal Ben-Israel who assisted in the

References

- Belmaker, R., Lazar, B., Stein, M., Taha, N., & Bookman, R. (2019). Constraints on aragonite precipitation in the Dead Sea from geochemical measurements of flood plumes. *Quaternary Science Reviews*, 221, 105876. <https://doi.org/10.1016/j.quascirev.2019.105876>
- Ben-Yosef, E., Millman, M., Shaar, R., Tauxe, L., & Lipschits, O. (2017). Six centuries of geomagnetic intensity variations recorded by royal Judean stamped jar handles. *Proceedings of the National Academy of Sciences*, 114, 2160–2165. <https://doi.org/10.1073/pnas.1615797114>
- Ben-Yosef, E., Tauxe, L., Levy, T. E., Shaar, R., Ron, H., & Najjar, M. (2009). Geomagnetic intensity spike recorded in high resolution slag deposit in Southern Jordan. *Earth and Planetary Science Letters*, 287, 529–539. <https://doi.org/10.1016/j.epsl.2009.09.001>
- Bloemendal, J., King, J. W., Hall, F. R., & Doh, S.-J. (1992). Rock magnetism of Late Neogene and Pleistocene deep-sea sediments: Relationship to sediment source, diagenetic processes, and sediment lithology. *Journal of Geophysical Research*, 97, 4361–4375. <https://doi.org/10.1029/91jb03068>
- Bookman, R., Enzel, Y., Agnon, A., & Stein, M. (2004). Late Holocene lake levels of the Dead Sea. *GSA Bulletin*, 116, 555–571. <https://doi.org/10.1130/B25286.1>

field. Eldad Hazan and all the rangers in the Ein-Feshkha Nature Reserve for the help and warm hospitality. To the anonymous reviewers who helped improve this manuscript. This study was supported by Israel Science Foundation grant No. 1364/15 to RS, the Dead Sea Deep Drill Center of Excellence (COE) of the Israel Science Foundation (grants # 1736/11 and 1436/14 to MS), the European Research Council (ERC) under the European Union's Horizon 2020 research and innovation program (grant agreement No. 804490).

Campuzano, S. A., Gómez-Paccard, M., Pavón-Carrasco, F. J., & Osete, M. L. (2019). Emergence and evolution of the South Atlantic Anomaly revealed by the new paleomagnetic reconstruction SHAWQ2k. *Earth and Planetary Science Letters*, *512*, 17–26. <https://doi.org/10.1016/j.epsl.2019.01.050>

Cariocchi, C., Sagnotti, L., Campuzano, S. A., Lucchi, R. G., Macri, P., Rebesco, M., & Camerlenghi, A. (2020). A refined age calibrated paleosecular variation and relative paleointensity stack for the NW Barents Sea: Implication for geomagnetic field behavior during the Holocene. *Quaternary Science Reviews*, *229*, 106133. <https://doi.org/10.1016/j.quascirev.2019.106133>

Constable, C., Korte, M., & Panovska, S. (2016). Persistent high paleosecular variation activity in southern hemisphere for at least 10 000 years. *Earth and Planetary Science Letters*, *453*, 78–86. <https://doi.org/10.1016/j.epsl.2016.08.015>

Ebert, Y., Shaar, R., Emmanuel, S., Nowaczyk, N., & Stein, M. (2018). Overwriting of sedimentary magnetism by bacterially mediated mineral alteration. *Geology*, *46*, 291–294. <https://doi.org/10.1130/g39706.1>

Ebert, Y., Shaar, R., Levy, E., Zhao, X., Roberts, A., & Stein, M. (2020). Magnetic properties of late Holocene Dead Sea sediments as a monitor of regional hydroclimate. *Geochemistry, Geophysics, Geosystems*, e2020GC009176. <https://doi.org/10.1029/2020GC009176>

Fisher, R. (1953). Dispersion on a sphere. *Proceedings of the Royal Society A: Mathematical, Physical and Engineering Sciences*, *217*, 295–305. <https://doi.org/10.1098/rspa.1953.0064>

Frank, U., Nowaczyk, N. R., & Negendank, J. F. W. (2007a). Palaeomagnetism of greigite bearing sediments from the Dead Sea, Israel. *Geophysical Journal International*, *168*, 904–920. <https://doi.org/10.1111/j.1365-246x.2006.03263.x>

Frank, U., Nowaczyk, N. R., & Negendank, J. F. W. (2007b). Rock magnetism of greigite bearing sediments from the Dead Sea, Israel. *Geophysical Journal International*, *168*, 921–934. <https://doi.org/10.1111/j.1365-246x.2006.03273.x>

Frank, U., Schwab, M. J., & Negendank, J. F. W. (2002). A lacustrine record of paleomagnetic secular variations from Birkat Ram, Golan Heights (Israel) for the last 4400 years. *Physics of the Earth and Planetary Interiors*, *133*(1), 21–34. [https://doi.org/10.1016/S0031-9201\(02\)00085-7](https://doi.org/10.1016/S0031-9201(02)00085-7)

Gallet, Y., & Al-Maqdissi, M. (2010). Archeomagnetism in Mishirfeh-Qatna: New data on the evolution of intensity in the earthly magnetic field in the Middle East during the last millennia. *Akkadica*, *131*, 29–46. Go to ISI>://WOS:000287672800003.

Gallet, Y., D'Andrea, M., Genevey, A., Pinnock, F., Le Goff, M., & Matthiae, P. (2014). Archeomagnetism at Ebla (Tell Mardikh, Syria). New data on geomagnetic field intensity variations in the Near East during the Bronze Age. *Journal of Archaeological Science*, *42*, 295–304. <https://doi.org/10.1016/j.jas.2013.11.007>

Gallet, Y., Genevey, A., & Courtillot, V. (2003). On the possible occurrence of 'archeomagnetic jerks' in the geomagnetic field over the past three millennia. *Earth and Planetary Science Letters*, *214*(1–2), 237–242. [https://doi.org/10.1016/S0012-821X\(03\)00362-5](https://doi.org/10.1016/S0012-821X(03)00362-5)

Gallet, Y., Genevey, A., Le Goff, M., Fluteau, F., & Ali Eshraghi, S. (2006). Possible impact of the Earth's magnetic field on the history of ancient civilizations. *Earth and Planetary Science Letters*, *246*, 17–26. <https://doi.org/10.1016/j.epsl.2006.04.001>

Gallet, Y., Le Goff, M., Genevey, A., Margueron, J., & Matthiae, P. (2008). Geomagnetic field intensity behavior in the Middle East between similar to 3000 BC and similar to 1500 BC. *Geophysical Research Letters*, *35*, L02307. <https://doi.org/10.1029/2007gl031991>

Garfunkel, Z. (1981). Internal structure of the Dead Sea leaky transform (rift) in relation to plate kinematics. *Tectonophysics*, *80*, 81–108. [https://doi.org/10.1016/0040-1951\(81\)90143-8](https://doi.org/10.1016/0040-1951(81)90143-8)

Genevey, A. S., Gallet, Y., & Margueron, J. C. (2003). Eight thousand years of geomagnetic field intensity variations in the eastern Mediterranean. *Journal of Geophysical Research*, *108*(B5), 2228. <https://doi.org/10.1029/2001jb001612>

Haliva-Cohen, A., Stein, M., Goldstein, S. L., Sandler, A., & Starinsky, A. (2012). Sources and transport routes of fine detritus material to the Late Quaternary Dead Sea basin. *Quaternary Science Reviews*, *50*, 55–70. <https://doi.org/10.1016/j.quascirev.2012.06.014>

Häusler, S., Weber, M., Siebert, C., Holtappels, M., Noriega-Ortega, B. E., De Beer, D., & Ionescu, D. (2014). Sulfate reduction and sulfide oxidation in extremely steep salinity gradients formed by freshwater springs emerging into the Dead Sea. *FEMS Microbiology Ecology*, *90*, 956–969. <https://doi.org/10.1111/1574-6941.12449>

Kagan, E. J., Stein, M., Agnon, A., & Ramsey, C. B. (2010). Paleoearthquakes as anchor points in Bayesian radiocarbon deposition models: A case study from the Dead Sea. *Radiocarbon*, *52*, 1018–1026. <https://doi.org/10.1017/S0033822200046105>

Kagan, E., Stein, M., Agnon, A., & Neumann, F. (2011). Intrabasin paleoearthquake and quiescence correlation of the late Holocene Dead Sea. *Journal of Geophysical Research*, *116*. <https://doi.org/10.1029/2010jb007452>

Kirschvink, J. L. (1980). The least-squares line and plane and the analysis of paleomagnetic data. *Geophysical Journal International*, *62*, 699–718. <https://doi.org/10.1111/j.1365-246x.1980.tb02601.x>

Korte, M., Donadini, F., & Constable, C. G. (2009). Geomagnetic field for 0–3 ka: 2. A new series of time-varying global models. *Geochemistry, Geophysics, Geosystems*, *10*(6). <https://doi.org/10.1029/2008GC002297>

Machlus, M., Enzel, Y., Goldstein, S. L., Marco, S., & Stein, M. (2000). Reconstructing low levels of Lake Lisan by correlating fan-delta and lacustrine deposits. *Quaternary International*, *73–74*, 137–144. [https://doi.org/10.1016/S1040-6182\(00\)00070-7](https://doi.org/10.1016/S1040-6182(00)00070-7)

Marco, S., Ron, H., McWilliams, M. O., & Stein, M. (1998). High-resolution record of geomagnetic secular variation from Late Pleistocene Lake Lisan sediments (paleo Dead Sea). *Earth and Planetary Science Letters*, *161*, 145–160. [https://doi.org/10.1016/S0012-821X\(98\)00146-0](https://doi.org/10.1016/S0012-821X(98)00146-0)

Migowski, C., Agnon, A., Bookman, R., Negendank, J. F. W., & Stein, M. (2004). Recurrence pattern of Holocene earthquakes along the Dead Sea transform revealed by varve-counting and radiocarbon dating of lacustrine sediments. *Earth and Planetary Science Letters*, *222*, 301–314. <https://doi.org/10.1016/j.epsl.2004.02.015>

Migowski, C., Stein, M., Prasad, S., Negendank, J. F. W., & Agnon, A. (2006). Holocene Climate Variability and Cultural Evolution in the Near East from the Dead Sea Sedimentary Record. *Quaternary Research*, *66*, 421–431. <https://doi.org/10.1016/j.yqres.2006.06.010>

Nilsson, A., Holme, R., Korte, M., Suttie, N., & Hill, M. (2014). Reconstructing Holocene geomagnetic field variation: New methods, models and implications. *Geophysical Journal International*, *198*, 229–248. <https://doi.org/10.1093/gji/ggu120>

Nishri, A., & Stiller, M. (1984). Iron in the Dead Sea. *Earth and Planetary Science Letters*, *71*, 405–414. [https://doi.org/10.1016/0012-821X\(84\)90106-7](https://doi.org/10.1016/0012-821X(84)90106-7)

Osete, M. L., Molina-Cardin, A., Campuzano, S. A., Aguilera-Arzo, G., Barrachina-Ibañez, A., Falomir-Granell, F., et al. (2020). Two archeomagnetic intensity maxima and rapid directional variation rates during the Early Iron Age observed at Iberian coordinates. Implications on the evolution of the Levantine Iron Age anomaly. *Earth and Planetary Science Letters*, *533*, 116047. <https://doi.org/10.1016/j.epsl.2019.116047>

Pavón-Carrasco, F. J., Osete, M. L., Torta, J. M., & De Santis, A. (2014). A geomagnetic field model for the Holocene based on archeomagnetic and lava flow data. *Earth and Planetary Science Letters*, *388*, 98–109. <https://doi.org/10.1016/j.epsl.2013.11.046>

Ramsey, C. B. (2008). Radiocarbon dating: Revolutions in understanding. *Archaeometry*, *50*, 249–275. <https://doi.org/10.1111/j.1475-4754.2008.00394.x>

Ramsey, C. B. (2009). Bayesian analysis of radiocarbon dates. *Radiocarbon*, *51*, 337–360. https://doi.org/10.2458/azu_js_rc.51.3494

- Ramsey, C. B. (2017). Methods for summarizing radiocarbon datasets. *Radiocarbon*, 59, 1809–1833. <https://doi.org/10.1017/rdc.2017.108>
- Reimer, P. J., Bard, E., Bayliss, A., Beck, J. W., Blackwell, P. G., Ramsey, C. B., et al. (2013). IntCal13 and Marine13 radiocarbon age calibration curves 0–50,000 years cal BP. *Radiocarbon*, 55, 1869–1887. https://doi.org/10.2458/azu_js_rc.55.16947
- Roberts, A. P. (1995). Magnetic properties of sedimentary greigite (Fe₃S₄). *Earth and Planetary Science Letters*, 134, 227–236. [https://doi.org/10.1016/0012-821x\(95\)00131-u](https://doi.org/10.1016/0012-821x(95)00131-u)
- Ron, H., Nowaczyk, N. R., Frank, U., Marco, S., & McWilliams, M. O. (2006). Magnetic properties of Lake Lisan and Holocene Dead Sea sediments and the fidelity of chemical and detrital remanent magnetization. *New frontiers in Dead Sea paleoenvironmental research* (401, p. 171). Geological Society of America. <https://doi.org/10.1130/SPE401>
- Rowan, C. J., & Roberts, A. P. (2006). Magnetite dissolution, diachronous greigite formation, and secondary magnetizations from pyrite oxidation: Unravelling complex magnetizations in Neogene marine sediments from New Zealand. *Earth and Planetary Science Letters*, 241, 119–137. <https://doi.org/10.1016/j.epsl.2005.10.017>
- Sagnotti, L., Roberts, A. P., Weaver, R., Verosub, K. L., Florindo, F., Pike, C. R., et al. (2005). Apparent magnetic polarity reversals due to remagnetization resulting from late diagenetic growth of greigite from siderite. *Geophysical Journal International*, 160, 89–100.
- Sagnotti, L., & Winkler, A. (1999). Rock magnetism and palaeomagnetism of greigite-bearing mudstones in the Italian peninsula. *Earth and Planetary Science Letters*, 165, 67–80. [https://doi.org/10.1016/s0012-821x\(98\)00248-9](https://doi.org/10.1016/s0012-821x(98)00248-9)
- Shaar, R., Bechar, S., Finkelstein, I., Gallet, Y., Martin, M. A., Ebert, Y., et al. (2020). Synchronizing geomagnetic field intensity records in the Levant between the 23rd and 15th centuries BCE: Chronological and methodological implications. *Geochemistry, Geophysics, Geosystems*, 21. <https://doi.org/10.1029/2020GC009251>
- Shaar, R., Ben-Yosef, E., Ron, H., Tauxe, L., Agnon, A., & Kessel, R. (2011). Geomagnetic field intensity: How high can it get? How fast can it change? Constraints from Iron Age copper slag. *Earth and Planetary Science Letters*, 301, 297–306. <https://doi.org/10.1016/j.epsl.2010.11.013>
- Shaar, R., Hassul, E., Raphael, K., Ebert, Y., Segal, Y., Eden, I., et al. (2018). The first catalog of archeomagnetic directions from Israel with 4,000 years of geomagnetic secular variations [original research]. *Frontiers of Earth Science*, 6. <https://doi.org/10.3389/feart.2018.00164>
- Shaar, R., Tauxe, L., Ben-Yosef, E., Kassianidou, V., Lorentzen, B., Feinberg, J. M., & Levy, T. E. (2015). Decadal-scale variations in geomagnetic field intensity from ancient Cypriot slag mounds. *Geochemistry, Geophysics, Geosystems*, 16, 195–214. <https://doi.org/10.1002/2014gc005455>
- Shaar, R., Tauxe, L., Goguitchaichvili, A., Davidze, M., & Licheli, V. (2017). Further evidence of the Levantine Iron Age geomagnetic anomaly from Georgian pottery. *Geophysical Research Letters*, 44, 2229–2236. <https://doi.org/10.1002/2016gl071494>
- Shaar, R., Tauxe, L., Ron, H., Ebert, Y., Zuckerman, S., Finkelstein, I., & Agnon, A. (2016). Large geomagnetic field anomalies revealed in Bronze to Iron Age archeomagnetic data from Tel Megiddo and Tel Hazor, Israel. *Earth and Planetary Science Letters*, 442, 173–185. <https://doi.org/10.1016/j.epsl.2016.02.038>
- Snowball, I. A. N., & Thompson, R. O. Y. (1990). A mineral magnetic study of Holocene sedimentation in Lough Catherine, Northern Ireland. *Boreas*, 19, 127–146. <https://doi.org/10.1111/j.1502-3885.1990.tb00574.x>
- Snowball, I. F. (1991). Magnetic hysteresis properties of greigite (Fe₃S₄) and a new occurrence in Holocene sediments from Swedish Lapland. *Physics of the Earth and Planetary Interiors*, 68, 32–40. [https://doi.org/10.1016/0031-9201\(91\)90004-2](https://doi.org/10.1016/0031-9201(91)90004-2)
- Snowball, I. F. (1997). Gyromagnetic magnetization and the magnetic properties of greigite-bearing clays in southern Sweden. *Geophysical Journal International*, 129, 624–636. <https://doi.org/10.1111/j.1365-246x.1997.tb04498.x>
- Speranza, F., Maritan, L., Mazzoli, C., Morandi Bonacossi, D., & D'Ajello Caracciolo, F. (2006). First directional archeomagnetic results from Syria: Evidence from Tell Mishrifeh/Qatna. *Geophysical Journal International*, 165, 47–52. <https://doi.org/10.1111/j.1365-246x.2006.02914.x>
- Stein, M., Starinsky, A., Katz, A., Goldstein, S. L., Machlus, M., & Schramm, A. (1997). Strontium isotopic, chemical, and sedimentological evidence for the evolution of Lake Lisan and the Dead Sea. *Geochimica et Cosmochimica Acta*, 61, 3975–3992. [https://doi.org/10.1016/s0016-7037\(97\)00191-9](https://doi.org/10.1016/s0016-7037(97)00191-9)
- Tauxe, L., Shaar, R., Jonestrask, L., Swanson-Hysell, N. L., Minnett, R., Koppers, A. A. P., et al. (2016). PmagPy: Software package for paleomagnetic data analysis and a bridge to the magnetics information consortium (MagIC) database. *Geochemistry, Geophysics, Geosystems*, 17, 2450–2463. <https://doi.org/10.1002/2016gc006307>
- Tauxe, L., & Staudigel, H. (2004). Strength of the geomagnetic field in the Cretaceous Normal Superchron: New data from submarine basaltic glass of the Troodos Ophiolite. *Geochemistry, Geophysics, Geosystems*, 5. <https://doi.org/10.1029/2003gc000635>
- Tema, E., Hedley, I., Fasnacht, W., & Peege, C. (2018). Insights on the geomagnetic secular variation in the Eastern Mediterranean: First directional data from Cyprus. *Physics of the Earth and Planetary Interiors*, 285, 1–11. <https://doi.org/10.1016/j.pepi.2018.10.001>
- Tema, E., Hedley, I., Pavón-Carrasco, F. J., Ferrara, E., Gaber, P., Pilides, D., et al. (2021). The directional occurrence of the Levantine geomagnetic field anomaly: New data from Cyprus and abrupt directional changes. *Earth and Planetary Science Letters*, 557, 116731. <https://doi.org/10.1016/j.epsl.2020.116731>
- Thompson, R., Turner, G. M., Stiller, M., & Kaufman, A. (1985). Near east paleomagnetic secular variation recorded in sediments from the Sea of Galilee (Lake Kinneret). *Quaternary Research*, 23, 175–188. [https://doi.org/10.1016/0033-5894\(85\)90027-4](https://doi.org/10.1016/0033-5894(85)90027-4)
- Vaknin, Y., Shaar, R., Gadot, Y., Shalev, Y., Lipschits, O., & Ben-Yosef, E. (2020). The Earth's magnetic field in Jerusalem during the Babylonian destruction: A unique reference for field behavior and an anchor for archeomagnetic dating. *PLoS One*, 15. <https://doi.org/10.1371/journal.pone.0237029>